Eur. Phys. J A **2**, 193–198 (1998)

THE EUROPEAN PHYSICAL JOURNAL A

Production of medium-weight isotopes by fragmentation in 750 A MeV ^{238}U on ^{208}Pb collisions

J. Benlliure[1], P. Armbruster[1], M. Bernas[2], C. Böckstiegel[3], S. Czajkowski[4], C. Donzaud[2], H. Geissel[1], A. Heinz[1], C. Kozhuharov[1], Ph. Dessagne[5], G. Münzenberg[1], M. Pfützner[1], C. Stéphan[2], K.-H. Schmidt[1], K. Sümmerer[1], W. Schwab[1], L. Tassan-Got[2], B. Voss[1]

[1] Gesellschaft für Schwerionenforschung, Planckstrasse 1, D-64291 Darmstadt, Germany
[2] IPN Orsay, BP 1, F-91406 Orsay Cedex, France
[3] Institut für Kernphysik, TU Darmstadt, Schloßgartenstr. 9, D-64289 Darmstadt, Germany
[4] Centre d'Etudes Nucléaires de Bordeaux-Gradignan, F-33175, Gradignan Cedex, France
[5] Centre de Recherche Nucléaire, Strasbourg, IN2P3, France

Received: 3 October 1997 / Revised version: 27 February 1998
Communicated by V. Metag

Abstract. Projectile fragmentation of ^{238}U in a lead target was investigated at a bombarding energy of 750 A MeV. Isotopic production cross sections of about 250 different projectile fragments in the element range Z = 30–53 were measured with the FRagment Separator (FRS). The magnetic selection and the kinematical analysis of the measured isotopes allowed to disentangle fission and fragmentation residues. The mass loss of these residues indicates a violent collision where a large amount of energy is dissipated. The position of the fragmentation corridor defined by the measured residues was used to determine an effective proton-evaporation barrier.

PACS. 25.75.-q – 25.70.Mn – 21.10.Ft – 21.10.Gv – 27.50.+e – 27.50.+j – 24.10.Pa

1 Introduction

In recent years, the fragmentation of heavy relativistic projectiles was studied at GSI both in inclusive experiments at the FRagment Separator FRS (see e.g. [1,2]) and in exclusive experiments at the ALADIN spectrometer [3]. In both cases, the emphasis was on studies of medium- and heavy-mass fragments which have velocities close to that of the beam.

The FRS allowed for a full isotopical identification with respect to both A and Z, but the experiments were restricted to fragmentation products close to the projectiles.

The ALADIN experiments, however, which covered a much wider mass range, only resolved the nuclear charge Z of the fragments. The mass resolution was not sufficient to identify individual isotopes for fragments with charge bigger than 10. Only a mean mass value for each element could be given [4]. In this case, as an estimate for the unknown mass distribution of a fragment with nuclear charge $Z \geq 10$, the ALADIN group has used [5] an empirical description for the most probable fragment mass of a given nuclear charge Z as parametrized by the EPAX formula [6]. The validity of this procedure has been checked for the mean mass value [4], but is not justified a priori for the whole mass distribution since the EPAX parametrization has been shown to be valid mainly for fragments with masses A larger than about half the mass of the projectile, A_p [6].

In the present work we present production cross sections for medium-mass fragments with atomic numbers $30 \leq Z \leq 53$ formed in collisions of 750 A MeV ^{238}U projectiles with lead target nuclei. These data complement similar measurements of heavy-mass residues [7,8] and of fission products [9–12]. The lower limits of fragment mass and charge numbers studied in the present work, about 0.3 A_p and 0.3 Z_p, respectively, allow to test the validity of the EPAX parametrization in a hitherto scarcely-explored region.

At the same time we study the A/Z ratio of fragmentation residues of ^{238}U in a region of nuclear charge Z which approaches the regime of multifragmentation. Thus, we can check experimentally if the intermediate-mass fragments IMF observed by the ALADIN experiments are formed by the same "abrasion-ablation" type reactions that form heavier fragments and if the calculation of their average A/Z ration by the EPAX formula is justified.

As a final topic we will investigate the "universality" of the position of the fragmentation-residue corridor [13], and how this position is related to the competition between neutron and proton evaporation.

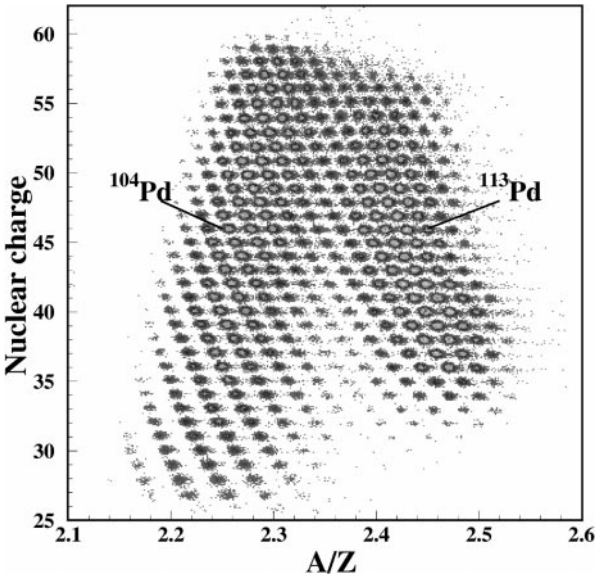

Fig. 1. Z − A/Z scatter plot of fission and fragmentation residues observed at Bρ= 0.90·(Bρ)$_o$ for the reaction ^{238}U(750 A MeV)+^{208}Pb

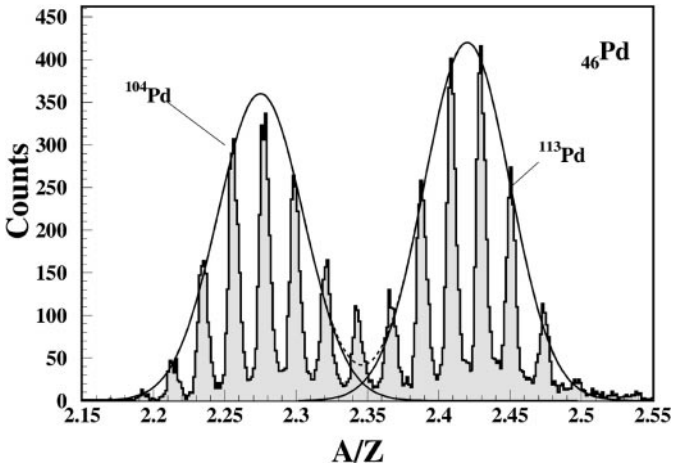

Fig. 2. A/Z identification of Pd isotopes observed at Bρ= 0.90·(Bρ)$_o$. The two observed regions correspond to fragmentation and backward fission. The *lines* represent Gaussian fits in order to estimate the contribution of fragmentation and backward fission in the measured yield of each isotope

2 The experiment

The experiment was performed at the heavy-ion synchrotron SIS at GSI, Darmstadt. A beam of 2·10^5 ^{238}U ions/s accelerated to 750 A MeV impinged on a lead target (1.26 g/cm^2), located at the entrance of the fragment separator FRS [14]. The beam intensity was measured with a secondary-electron current monitor. The FRS was operated as an achromat in order to achieve isotopic separation of the reaction products. The identification in mass and charge is based on measurements of the magnetic rigidity, time of flight and energy loss for each fragment passing through the FRS (see [10] for a schematic representation of the detectors used). Two position-sensitive plastic scintillators located in the intermediate and in the final focal plane, respectively, provide the time-of-flight (ToF) and magnetic-rigidity measurements. The nuclear charge Z was obtained by means of the energy loss measured in a four-stage ionization chamber at the exit of the FRS.

The charge and mass calibrations were extrapolated from the energy loss, Bρ, and ToF calibration for ^{238}U. Both calibrations were confirmed by finding the well established enhanced yields for Zr and Te, and for the N=82 nucleus, ^{134}Te, observed in the low-energy fission process measured at magnetic rigidities larger than that of the beam [9].

The fragmentation residues were detected at three tunings of the fragment separator corresponding to magnetic rigidities smaller by 10%, 14%, and 18% than the magnetic rigidity of the beam, (Bρ)$_o$. In Fig. 1, we show as an example the isotopic identification matrix measured at a magnetic rigidity of 0.90·(Bρ)$_o$. The two groups of isotopes visible in this picture can be interpreted from their kinematical properties [12]. Taking into account the magnetic rigidity and the different A/Z values, we attribute these groups to fragmentation (left hand) and to fission (right hand) of ^{238}U with the fission fragments emitted in backward direction.

From the fission kinematics discussed e.g. in [10], it is obvious that at 0.90·(Bρ)$_o$ only fission products emitted in backward direction with respect to the ^{238}U beam can be observed. The particular selection of isotopes visible in Fig. 1 is due to the FRS momentum acceptance of ±1% [14] around 0.90·(Bρ)$_o$.

In Fig. 2 we present a projection of Fig.1 onto the A/Z-axis for Z=46 (Pd). The two groups are well separated and clearly visible. To extract the relative amount of the fragmentation cross section in the overlap region, the maxima of the peaks were fitted with Gaussians (disregarding odd-even effects) and the peak areas of $^{107-109}$Pd were divided according to the ratio of the two Gaussians.

3 Results

In order to determine the fragmentation cross sections, several corrections must be applied. The main correction is due to the transmission of the fragments through the FRS. In the case of fragmentation residues at relativistic energies, the angular aperture of the spectrometer is large enough, and the only limitation to the acceptance is due to the broad momentum distributions (≈ 6%) of the produced residues compared with the 2% momentum acceptance of the spectrometer. The transmission was estimated by ion-optical calculations. In order to describe the kinematics of the reaction we used the average longitudinal momentum deduced from our data. The width of the momentum distribution is firstly determined by the energy loss in the target. The additional contribution to this width due to the reaction was assumed to follow the Morrissey systematics [15]. The magnitude of this second contribution is not crucial for determining the ion-optical

transmission since the first contribution due to the energy loss, which can be reliably calculated, represents the major part of the momentum width. Energy losses in the ToF scintillator detectors were taken into account also. We corrected for the dead time of the data acquisition which varied from 5% to 20%, depending on the counting rate. Losses of fragments by secondary reactions in the target and in the intermediate-focus plastic scintillator were corrected by using empirical total reaction cross sections [17]. These losses were calculated to be $\approx 12\%$. All fragments were fully stripped, contributions from other ionic charge states were calculated to be below 1%. The values for the total transmission for fragmentation residues through the FRS are in the range of 20-70%.

Production cross sections of about 250 fragmentation products were measured for atomic numbers between Z=30 and Z=53. They are shown in Fig. 3. These isotopic distributions are characterized by maxima shifted to the neutron-deficient side of the valley of β-stability. We can observe that the slopes at the two sides of the distributions are different leading to higher production cross sections of the neutron-rich isotopes.

4 Discussion

4.1 Comparison with an empirical parametrization

In Fig. 3, the solid lines correspond to calculations performed with the empirical formula EPAX [6]. The EPAX formula is a parametrization of measured production cross sections from target and projectile fragmentation and was estimated to be valid for fragment masses $40 \leq A \leq 200$ down to roughly half the mass of the projectile ($A/A_p \leq 0.5$).

Apart from a narrow range of isotopes near the projectile ($A/A_p \geq 0.86$), the shapes of the isotopic distributions depend only on the fragment mass A, independent of A_p. As we will discuss later, this independence is related to the fact that the isotopic distributions are produced by statistical decay processes from fully equilibrated prefragments formed in the first (abrasion) step of the high-energy reaction [3].

This parametrization provides a good description of our experimental data since shapes, position of the maxima and absolute cross sections of the isotopic distributions are indeed well reproduced by the formula. Only some deviations are observed in the production cross section for the neutron-rich isotopes of the heaviest measured elements. It can not be excluded that these deviations originate from an overestimation of the transmission evaluations for these isotopes which are located on the edge of the final focal plane detector of the spectrometer.

Furthermore, the EPAX parametrization seems to be valid even for isotopes with $A/A_p \leq 0.3$. This is an additional proof that the use of the EPAX parametrization to estimate average fragment masses from measured fragment charge numbers (as was done for the analysis of spectator fragmentation in the ALADIN experiments [5]) is valid.

4.2 Proton evaporation barriers

From the EPAX parametrization we deduce that the location of the fragmentation-residue corridor [13], the line connecting the maximum isotopic yields of each nuclear charge Z produced in fragmentation reactions, is a rather universal line on the chart of the nuclides. With the exception of the elements close to the projectile, this line does not depend on the composition of the reaction partners. This finding suggests that the fragmentation corridor is insensitive to the earlier stages of the reaction but it is rather defined by the properties of the last steps of the deexcitation chain [4]. As we will see, the position of the fragmentation-residue corridor is sensitively determined by the magnitude of the Coulomb barrier for the evaporation of protons. This quantity can thus be extracted from the data.

In general, the formation of fragmentation residues from the projectile is a violent process. These reactions are considered to proceed in two steps: first a fast abrasion step, leaving the fireball and the excited spectators [18–20]; then a slow ablation step in which the spectators equilibrate and finally deexcite by evaporating particles. For heavy nuclei, also fission is important. Campi and Hüfner [21] have interpreted the evaporation stage as a diffusion process which tends to develop versus an equilibrium in the isospin degree of freedom. This model has been elaborated further by Gaimard and Schmidt [20].

The characteristics of the diffusion process can be understood in the following way: during the evaporation process, neutron emission will be favored over proton emission when starting from stable isotopes by the absence of the Coulomb barrier, so that the maxima of the residue yields will lie on the neutron-deficient side of the valley of β-stability. The local slope of the fragmentation corridor in the Z − N plane ($\Delta N/\Delta Z$) is determined by the competition between different particles during the last steps of the deexcitation chain of a hot nucleus. If the consideration is restricted to the evaporation of neutrons and protons, which are the most abundantly emitted particles at low energies, and if angular-momentum effects are disregarded, this local competition between neutron and proton evaporation can be written in terms of the statistical model as:

$$\frac{\Gamma_n}{\Gamma_p} \approx \frac{exp[2\sqrt{a(E-\langle B_n\rangle)}]}{exp[2\sqrt{a(E-\langle B_p\rangle - E_c)}]} \qquad (1)$$

where a is the level-density parameter, E is the excitation energy of the nucleus, $\langle B_n\rangle$ and $\langle B_p\rangle$ are the neutron and proton binding energies calculated with even-odd effects averaged out as proposed in reference [22]. E_c is an effective proton-evaporation barrier which takes into account the barrier transmission. This barrier can be calculated by using a function which retains the form of a simple Coulomb potential:

$$E_c = \frac{1.44(Z-1)}{1.22(A-1)^{1/3}+R} \qquad (2)$$

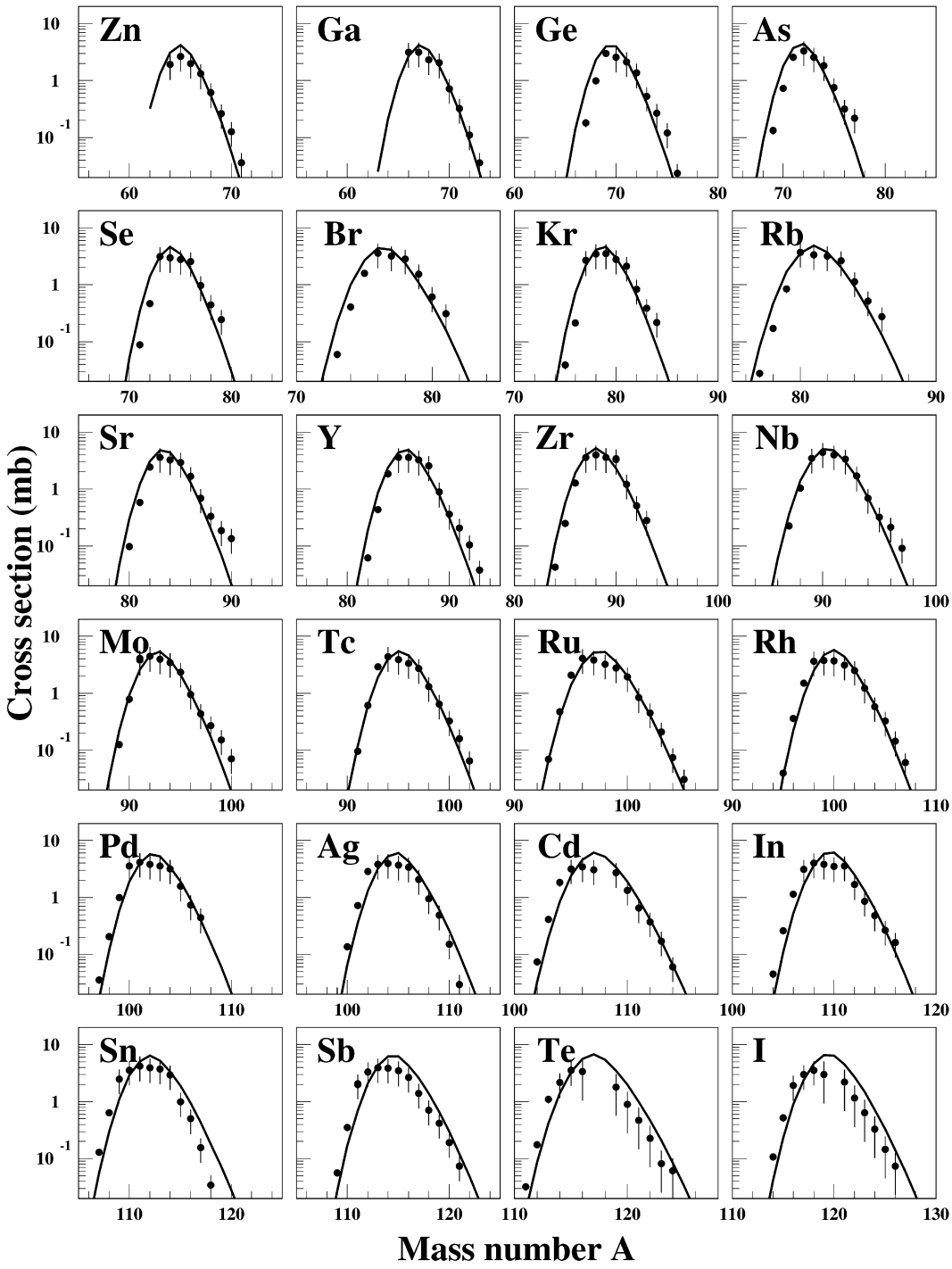

Fig. 3. Isotopic fragmentation cross sections of the reaction ^{238}U(750 A MeV)+^{208}Pb. The *solid lines* correspond to the result of a calculation with the EPAX formula

where Z and A are the atomic and mass number of the emitting system and R is the effective proton-evaporation radius.

Equating the right-hand side of (1) with the measured slope of the fragmentation corridor in the Z − N plane (ΔN/ΔZ), and choosing the excitation energy of the nucleus during the last steps of the deexcitation chain, we can calculate the isotopes populating the maximum of the evaporation corridor as a function of the effective proton-evaporation radius R. Comparing the calculated and the measured positions in the Z − N plane of the evaporation corridor we can determine the effective proton-evaporation radius R.

In Fig. 4, we show the measured positions of the isotopes produced with the highest cross section in the N/Z − Z plane (square symbols). The structure observed

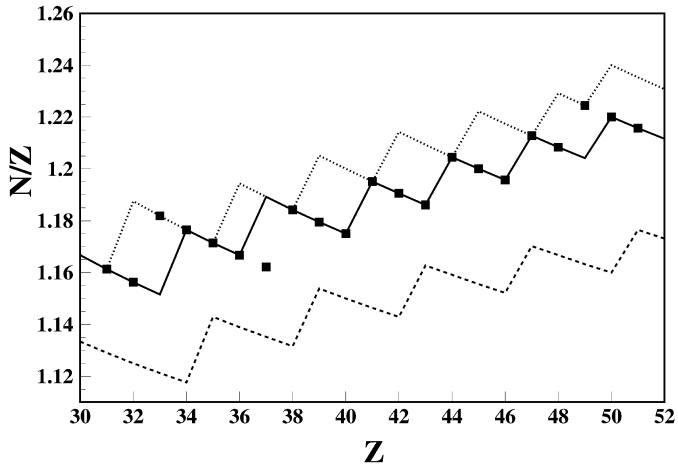

Fig. 4. N/Z value of the maximum isotopic yield as a function of its atomic charge. The experimental data are represented by the *solid square symbols*, and the *lines* show the results of three calculations assuming different effective proton-evaporation barriers (see text)

in this figure is due to the integer mass and charge values. The measured positions are compared with the calculated ones assuming an excitation energy of 30 MeV and three different effective radii for the proton evaporation: R = 4 fm (dashed line), R = 6 fm (solid line) and R = 8 fm (dotted line). These results depend weakly on the excitation energy, and in the range $20 \leq E \leq 40$ MeV the best agreement is obtained for $R = 6 \pm 0.5$ fm.

The effective proton-evaporation barriers calculated with R = 6 fm agree with the effective barriers proposed in [20]. The values estimated previously by Dostrovsky et al. [23] are higher by about 20%. Recently, effective proton evaporation barriers have been given [24] which are even larger by more than 30% than those proposed here.

Our results are lower by about 20% than the systematics of fusion barriers obtained by L.C. Vaz and J.M. Alexander [25]. This can be understood as a consequence of the tunneling which allows the emission of protons below the potential barrier which is effectively included in (2). The reduction of the effective evaporation barriers with respect to the systematics of fusion barriers should not be confounded with a possible general difference between evaporation and fusion barriers, as claimed by some authors [25–27], which could not be confirmed in other works [28,29]. The answer to this controversial question needs more elaborate theoretical calculations which would exceed the aim of this work.

The present work has given reliable values of effective barriers to be used in evaporation codes which can not afford for the computational effort of calculating transmission coefficients when they are applied in a very complex environment.

5 Conclusion

Inverse-kinematic reactions at relativistic energies have been used to study the isotope production in fragmentation reactions by using a zero-degree spectrometer. The qualitative description of the reaction mechanism leading to the formation of these residues allows to conclude that this experimental approach can also give new insight into the deexcitation mechanism involved in violent collisions. In addition, this experimental method also represents a suitable method for the production and study of neutron-deficient nuclei.

The good description of our data with EPAX gives confidence in the use of this parametrization to estimate average fragment masses from measured fragment charge numbers. The agreement between our data and this parametrization also suggests a rather universal behavior of the fragmentation-residue corridor. This universal behavior can be understood within the assumption that the location of the fragmentation-residue corridor is insensitive to the earlier stages of the reaction and then does not depend on the composition of the reaction partners.

Using the slope of the fragmentation corridor, determined mainly by the competition between proton and neutron evaporation on the last steps of the deexcitation chain, we calculated an effective proton-evaporation barrier assuming a statistical evaporation model. The calculated proton-evaporation barriers were found to be lower than the ones obtained from fusion-barrier systematics. This reduction is qualitatively expected because the calculated effective barriers include the effect of barrier transmission.

The above results, together with others concerning the production of residues close to the projectile [7], and the production of fission residues [11,12], demonstrate that the present experimental method also opens an efficient way to study all processes which take place in collisions of 1 GeV protons with lead or actinide targets and to measure the cross sections needed for the incineration of nuclear waste by means of hybrid reactors [30,31].

References

1. K.-H. Schmidt, T. Brohm, H.-G. Clerc, M. Dornik, M. Fauerbach, H. Geissel, A. Grewe, E. Hanelt, A. Junghans, A. Magel, W. Morawek, G. Münzenberg, F. Nickel, M. Pfützner, C. Scheidenberger, K. Sümmerer, D. Vieira, B. Voss and C. Ziegler, Phys. Lett. B**300** (1993) 313
2. E. Hanelt, A. Grewe, K.-H. Schmidt, T. Brohm, H.-G. Clerc, M. Dornik, M. Fauerbach, H. Geissel, A. Magel, G. Münzenberg, F. Nickel, M. Pfützner, C. Scheidenberger, M. Steiner, K. Sümmerer, B. Voss, M. Weber, J. Weckenmann and C. Ziegler, Z. Phys. A**346** (1993) 43
3. A. Schüttauf, W.D. Kunze, A. Wörner, M. Begemann-Blaich, Th. Blaich, D.R. Bowman, R.J. Charity, A. Cosmo, A. Ferrero, C.K. Gelbke, C. Grossß, W.C. Hsi, J. Hubele, G. Immé, I. Iori, J. Kempter, P. Kreutz, G.J. Kunde, V. Lindenstruth, M.A. Lisa, W.G. Lynch, U. Lynen, M. Mang, T. Möhlenkamp, A. Moroni, W.F.J. Müller, M. Neumann, B. Ocker, C.A. Ogilvie, G.F. Peaslee, J.

Pochodzalla, G. Raciti, F. Rosenberger, Th. Rubehn, H. Sann, C. Schwarz, W. Seidel, V. Serfling, L.G. Sobotka, J. Stroth, L. Stuttge, S. Tomasevic, W. Trautmann, A. Trzcinski, M.B. Tsang, A. Tucholski, G. Verde, C.W. Williams, E. Zude and B. Zwieglinski, Nucl. Phys. A**607** (1996) 457
4. A.S. Botvina, I.N. Mishustin, M. Begemann-Blaich, J. Hubele, G. Immé, I. Iori, P. Kreutz, G.J. Kunde, W.D. Kunze, V. Lindenstruth, U. Lynen, A. Moroni, W.F.J. Müller, C.A. Ogilvie, J. Pochodzalla, G. Raciti, Th. Rubehn, H. Sann, A. Schüttauf, W. Seidel, W. Trautmann, A. Wörner, Nucl. Phys. A**584** (1995) 737
5. J. Pochodzalla, T. Möhlenkamp, T. Rubehn, A. Schüttauf, A. Wörner, E. Zude, M. Begemann-Blaich, Th. Blaich, H. Emling, A. Ferrero, C. Groß, G. Immé, I. Iori, V. Lindenstruth, U. Lynen, A. Moroni, W.F.J. Müller, B. Ocker, G. Raciti, H. Sann, C. Schwarz, W. Seidel, V. Serfling, J. Stroth, W. Trautmann, A. Trzcinski, A. Tucholski, G. Verde and B. Zwieglinski, Phys. Rev. Lett. **75** (1995) 1040
6. K. Sümmerer, W. Brüchle, D.J. Morrisey, M. Schädel, B. Szweryn and Yang Weifan, Phys. Rev. C**42** (1990) 2546
7. H.-G. Clerc, M.de Jong, T. Brohm, M. Dornik, A. Grewe, E. Hanelt, A. Heinz, A. Junghans, C. Röhl, S. Steinhäuser, B. Voss, C. Ziegler, K.-H. Schmidt, S. Czajkowski, H. Geissel, H. Irnich, A. Magel, G. Münzenberg, F. Nickel, A. Piechaczek, C. Scheidenberger, W. Schwab, K. Sümmerer, W. Trinder, M. Pfütner, B. Blank, A. Ignatyuk, G. Kudyaev, Nucl. Phys. A**590** (1995) 785
8. T. Aumann, A. Grewe, K.-H. Schmidt, T. Brohm, H.-G. Clerc, M. Dornik, M. Fauerbach, H. Geissel, A. Magel, G. Münzenberg, F. Nickel, M. Pfützner, C. Scheidenberger, M. Steiner, K. Sümmerer, B. Voss, M. Weber, J. Weckenmann and C. Ziegler, Z. Phys. A**352** (1995) 163
9. M. Bernas, S. Czajkowski, P. Armbruster, H. Geissel, Ph. Dessagne, C. Donzaud, H.-R. Faust, E. Hanelt, A. Heinz, M. Hesse, C. Kozhuharov, Ch. Miehe, G. Münzenberg, M. Pfützner, C. Röhl, K.-H. Schmidt, W. Schwab, C. Stéphan, K. Sümmerer, L. Tassan-Got and B. Voss, Phys. Lett. B**331** (1994) 19
10. P. Armbruster, M. Bernas, S. Czajkowski, H. Geissel, T. Aumann, Ph. Dessagne, C. Donzaud, E. Hanelt, A. Heinz, M. Hesse, C. Kozhuharov, Ch. Miehe, G. Münzenberg, M. Pfützner, C. Röhl, K.-H. Schmidt, W. Schwab, C. Stéphan, K. Sümmerer, L. Tassan-Got and B. Voss, Z. Phys. A**355** (1996) 191
11. C. Donzaud, S. Czajkowski, P. Armbruster, M. Bernas, Ph. Dessagne, H. Geissel, E. Hanelt, A. Heinz, M. Hesse, C. Kozhuharov, Ch. Miehe, G. Münzenberg, M. Pfützner, C. Röhl, K.-H. Schmidt, W. Schwab, C. Stéphan, K. Sümmerer, L. Tassan-Got and B. Voss, Eur. Phys. J A**1** (1997) 407
12. W. Schwab, M. Bernas, P. Armbruster, S. Czajkowski, Ph. Dessagne, C. Donzaud, , H. Geissel, E. Hanelt, A. Heinz, M. Hesse, C. Kozhuharov, Ch. Miehe, G. Münzenberg, M. Pfützner, C. Röhl, K.-H. Schmidt, W. Schwab, C. Stéphan, K. Sümmerer, L. Tassan-Got and B. Voss, accepted by Euro. Phys. J. A
13. J.P. Dufour, H. Delagrange, R. Del Moral, A. Fleury, F. Hubert, Y. Llabador, M.B. Mauhourat, K.H. Schmidt and A. Lleres, Nucl. Phys. A**387** (1982) 157c
14. H. Geissel, P. Armbruster, K.-H. Behr, A. Brünle, K. Burkard, M. Chen, B. Franczak, H. Keller, O. Klepper, B. Langenbeck, F. Nickel, E. Pfeng, M. Pfützner, E. Roeckel, K. Rykaczewsky, I. Schall, D. Schardt, C. Scheidenberger, K.-H. Schmidt, A. Schröter, T. Schwab, K. Sümmerer, M. Weber, G. Münzenberg, T. Brohm, H.-G. Clerc, M. Fauerbach, J.-J. Gaimard, A. Grewe, E. Hanelt, B. Knödler, M. Steiner, B. Voss, J. Weckenmann, C. Ziegler, A. Magel, H. Wollnik, J.-P. Dufour, Y. Fujita, D.J. Vieira and B. Sherril, Nucl. Instrum. Methods B**70** (1992) 286
15. D.J. Morrissey, Phys. Rev. C 39 (1989) 460
16. M. Weber, C. Donzaud, J.P. Dufour, H. Geissel, A. Grewe, D. Guillemaud-Mueller, H. Keller, M. Lewitowicz, A. Magel, A.C. Mueller, G. Münzenberg, F. Nickel, M. Pfütner, A. Piechaczek, M. Pravikoff, E. Roeckl, K. Rykaczewski, M.G. Saint-Laurent, I. Schall, C. Stéphan, K. Sümmerer, L. Tassan-Got, D.J. Vieira, B. Voss, Nucl. Phys. A**578** (1994) 659
17. S. Kox, A. Gamp, C. Perrin, J. Arvieux, R. Bertholet, J.F. Bruandet, M. Buenerd, R. Cherkaoui, A.J. Cole, Y. El-Masri, N. Longequeue, J. Menet, F. Merchez, J.B. Viano, Phys. Rev. C**35** (1987) 1678
18. R. Serber, Phys. Rev. **72** (1947) 1114
19. J.D. Bowman, W.J. Swiatecki and C.E. Tsang, Lawrence Berkeley Report LBL-2908 (1973)
20. J.-J. Gaimard and K.-H. Schmidt, Nucl. Phys. A**531** (1991) 709
21. X. Campi, J. Hüfner, Phys. Rev. C**24** (1981) 2199
22. V.M. Kupriyanov, G.N. Smirenkin and B.I. Fursov, Sov. J. Nucl. Phys. **39** (1984) 176
23. I. Dostrovsky, Z. Fraenkel, G. Friedlander, Phys. Rev. **116** (1959) 683
24. R.J. Charity, M.A. McMahan, G.J. Wozniak, R.J. McDonald, L.G. Moretto, D.G. Sarantites, L.G. Sobotka, G. Guarino, A. Pantaleo, L. Fiore, A. Gobbi and K.D. Hildenbrand Nucl. Phys. A**483** (1988) 371
25. L.C. Vaz and J.M. Alexander, Z. Phys. A**318** (1984) 231
26. J.M. Alexander, D. Guerreau, L.C. Vaz, Z. Phys. A**305** (1982) 313
27. G. La Rana, D.J. Moses, W.E. Parker, M. Kaplan, D. Logan, R. Lacey, J.M. Alexander, R.J. Welberry, Phys. Rev. C**35** (1987) 373
28. I.M. Govil, J.R. Huizenga, W.U. Schröder, J. Tõke, Phys. Lett. B**197** (1987) 515
29. U. Gollerthan, T. Brohm, H.-G. Clerc, E. Hanelt, M. Horz, W. Morawek, W. Schwab, K.-H. Schmidt, F.P. Hessberger, G. Münzenberg, V. Ninov, R.S. Simon, J.P. Dufour, M. Montoya, Z. Phys. A**338** (1991) 51
30. C.D. Bowman, E.D. Arthur, P.W. Lisowski, G.P. Lawrence, R.J. Jensen, J.L. Anderson, B. Blind, M. Cappiello, J.W. Davidson, T.R. England, L.N. Engel, R.C. Haight, H.G. Hughes III, J.R. Ireland, R.A. Krakowski, R.J. LaBauve, B.C. Letellier, R.T. Perry, G.J. Russell, K.P. Staudhammer, G. Versamis, W.B. Wilson, Nucl. Instrum. Methods A**320** (1992) 336
31. C. Rubbia, J.A. Rubio, S. Buono, F. Carminati, N. Fiétier, J. Galvez, C. Gelès, Y. Kadi, R. Klapisch, P. Mandrillon, J.P. Revol, Ch. Roche, CERN report CERN/AT/95-44(ET)